OPEN JOURNAL SYSTEMS
ISSN:2237-2202

Available on line at Directory of Open Access Journals
Journal of Hyperspectral Remote Sensing v.12, n.4 (2022) 154-165

www.periodicos.ufpe.br/revistas/jhrs

Journal of Hyperspectral Remote Sensing
www.ufpe.br/jhrs

Use of NASA's AVIRIS-NG imagery for environmental mapping at the Rio Tinto mining district, southwestern Spain

Enton Bedini*, Josicleda Domiciano Galvíncio**, Jiang Chen***

*International Institute of Geoinformation Science and Earth Observation (ITC), Enschede, The Netherlands. Email: enton_bedini@hotmail.com. (Corresponding author).
**Universidade Federal de Pernambuco, Recife, Brazil. Email: josicleda.galvincio@ufpe.br.
***Shenyang Institute of Geology and Mineral Resources, CGS, Shenyang, Liaoning, 110034, China. Email: chen07761@itc.nl.

Received 9 March 2020; accepted 9 Jun 2022

Abstract

Airborne hyperspectral imagery recorded by the NASA's Next Generation Advanced Visible/Infrared Imaging Spectrometer (AVIRIS-NG) was analyzed for environmental mapping of the Rio Tinto mining district in southwestern Spain. The Rio Tinto mining district contains a giant world-class polymetallic sulfide deposit that has been mined from the antiquity to the modern times. The mining and ore processing activities have created large areas covered by sulfide-bearing mine waste, tailings, flooded open pits, slags, galleries and other mining facilities. The sulfide-bearing mine waste generates acid mine drainage (AMD) that contaminates the fluvial network. The Rio Tinto River is one of most AMD contaminated rivers in the world. Many secondary minerals associated with sulfide-bearing mine waste have diagnostic reflectance spectra due to absorptions of ferric and ferrous iron, water and hydroxyl. The mapping of the surface distribution of these secondary minerals is useful for environmental studies. The AVIRIS-NG radiance data were converted to surface reflectance using the Fast Line-of-sight Atmospheric Analysis of Hypercubes model. The AVIRIS-NG imagery was analyzed using the spectral mixture analysis. The AVIRIS-NG accurately mapped acid water, jarosite, goethite, hematite, melanterite, rozenite, copiapite, gypsum, undifferentiated metal sulfate hydrates, sericite and kaolinite. Acid waters occur in the tailings ponds, in the Rio Tinto River, and in various other locations within the study area. Jarosite, goethite and hematite are the predominant secondary iron minerals in the areas covered by sulfide-bearing mine waste. These secondary iron minerals are indicators of acid mine drainage generation. In few locations were distinguished from the AVIRIS-NG data the mineral melanterite and its dehydration product rozenite. The study gives new information on the surface distribution of environmentally important secondary iron minerals in the Rio Tinto mining district in southwestern Spain. The mapping results produced by the analysis of the AVIRIS-NG data can be useful to the environmental studies concerned with the pollution from acid mine drainage of the fluvial network of the area.
Keywords: Rio Tinto mining district, sulfides, mine waste, acid mine drainage, AVIRIS-NG.

Uso de imagens AVIRIS-NG da NASA para mapeamento ambiental no distrito de mineração de Rio Tinto, sudoeste da Espanha

Resumo

As imagens hiperespectrais aerotransportadas registradas pelo espectrômetro avançado de imagens visíveis/infravermelhas da NASA (AVIRIS-NG) foram analisadas para o mapeamento ambiental do distrito de mineração de Rio Tinto, no sudoeste da Espanha. O distrito de mineração de Rio Tinto contém um gigantesco depósito de sulfeto polimetálico de classe mundial que foi extraído desde a antiguidade até os tempos modernos. As atividades de mineração e processamento de minério criaram grandes áreas cobertas por resíduos de mineração contendo sulfeto, rejeitos, minas a céu aberto inundadas, escórias, galerias e outras instalações de mineração. Os rejeitos de mineração contendo sulfetos geram drenagem ácida de mina (DAM) que contamina a rede fluvial. O rio Rio Tinto é um dos rios mais contaminados pela AMD no mundo. Muitos minerais secundários associados com rejeitos de mina contendo sulfetos têm espectros de refletância diagnósticos devido a absorções de ferro férrico e ferroso, água e hidroxila. O mapeamento da distribuição superficial desses minerais secundários é útil para estudos ambientais. Os dados de radiância do AVIRIS-NG foram convertidos em refletância de superfície usando o modelo de Análise Atmosférica de Linha de Visão Rápida de Hipercubos. As imagens do AVIRIS-NG foram analisadas usando a análise de mistura espectral. O AVIRIS-

NG mapeou com precisão água ácida, jarosita, goethita, hematita, melanterita, rozenita, copiapita, gesso, hidratos de sulfato de metal indiferenciado, sericita e caulinita. Águas ácidas ocorrem nas lagoas de rejeitos, no rio Rio Tinto e em vários outros locais dentro da área de estudo. Jarosita, goetita e hematita são os minerais de ferro secundários predominantes nas áreas cobertas por rejeitos de mineração contendo sulfetos. Esses minerais de ferro secundários são indicadores de geração de drenagem ácida de mina. Em poucos locais foram distinguidos dos dados do AVIRIS-NG o mineral melanterita e seu produto de desidratação rozenita. O estudo fornece novas informações sobre a distribuição superficial de minerais de ferro secundário de importância ambiental no distrito de mineração de Rio Tinto, no sudoeste da Espanha. Os resultados do mapeamento produzidos pela análise dos dados do AVIRIS-NG podem ser úteis para os estudos ambientais relacionados com a poluição por drenagem ácida de mina da rede fluvial da área.

1. Introduction

The Rio Tinto volcanogenic massive sulfide deposit in southwestern Spain is a giant world-class polymetallic sulfide deposit (e.g., Pascual et al., 2021). The Rio Tinto ore deposit occurs in a volcanogenic sedimentary complex of Devonian-Carboniferous age that consists of dacites, basalts and layers of a phyllite sequence. The Rio Tinto ore deposit has been mined for copper, zinc, lead, gold, silver, etc., since before the Roman times and the mining activities continue to the present days (Olías and Nieto, 2015).

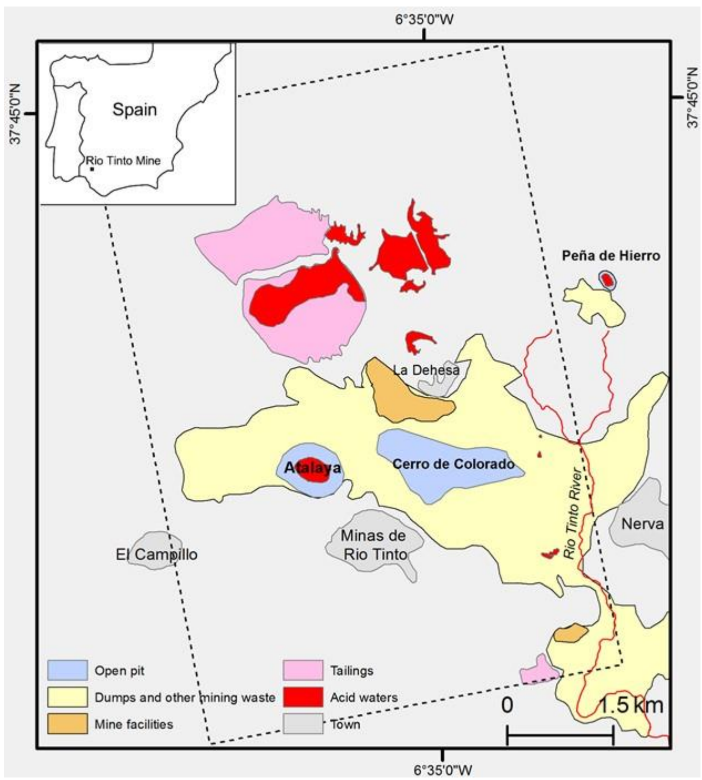

Figure 1. Schematic map of the Rio Tinto mining district in southwestern Spain (modified from Olías et al., 2020). The dashed black line shows the approximate spatial extent of AVIRIS-NG data analyzed in this study.

The ore extraction and processing at the Rio Tinto mining district has created large areas covered by waste dumps, tailings, flooded open pits, slags, galleries and other mining facilities (Figure 1). The weathering of sulfides (pyrite, pyrrhotite, etc.) in the surface, generates considerable acid mine drainage (AMD) that gives the characteristic red color to the Rio Tinto River (Figure 2; Olías et al., 2020). The mining of sulfide ores is an AMD pollution source of the fluvial network (e.g., de la Torre et al., 2010; Elghali et al., 2018; Olías et al., 2011; Olías et al., 2020; Cánovas et al., 2021; Córdoba et al., 2022). The Rio Tinto River represents one of the most AMD contaminated rivers in the world (Olías et al., 2020). The water of the Rio Tinto River has a pH close to 2.5 and high concentrations of pollutants (Olías et al., 2020). It is estimated that the AMD from the Rio Tinto mining district will continue for hundreds of years (Young, 1997).

Figure 2. The Rio Tinto River in southwestern Spain, heavily contaminated by acid mine drainage, flowing quietly toward the Atlantic Ocean (Photo courtesy of mundoshispanicos.com. Used with permission). Note the deep red color of the water.

The Rio Tinto mining district in southwestern Spain has also attracted the attention of researchers as an environment similar to some areas in the planet Mars (e.g., Roach et al., 2006; Amils et al., 2007; Sobron et al., 2014; Rull et al., 2021). Knowledge on the spectroscopic properties of analog terrestrial mineral associations are useful to develop criteria and detect similar environments on Mars (Roach et al., 2006).

The iron and sulfur driven environment at Rio Tinto mining district with its characteristic mineralogy composed of iron sulfates and iron hydroxides and oxides is of particular interest for planetary studies (Buckby et al., 2003; Fernández-Remolar, 2005; Amils et al., 2007). The Rio Tinto mining district has the potential to clarify some of the Martian mineralogic observations and provide a testing site for recognizing similar settings on Mars (e.g., Roach et al., 2006).

The reflectance spectroscopy is useful for the identification of infrared-active minerals (Clark, 1999). The hyperspectral technology or "imaging spectroscopy" acquires reflectance spectra by scanning large areas. In this way, it makes possible the production of environmental maps of surface composition (e.g., Goetz, 2009). The hyperspectral technology has found wide application in terrestrial and planetary mineralogical studies (e.g., Kruse et al., 2012; Carter et al., 2013; Liu et al., 2016; Bedini, 2017). A number of studies have applied the hyperspectral imagery to environmental mapping (e.g., Swayze et al., 2000; Antón-Pacheco et al., 2001; Choe et al., 2008; Riaza et al., 2011; Riaza et al., 2015; Kopačková and Hladíková, 2014; Zabcic et al., 2014; Farrand and Bhattacharya, 2021).

The NASA's Advanced Visible/Infrared Imaging Spectrometer (AVIRIS) records airborne hyperspectral data in the 0.35-2.5 μm wavelength region (e.g., Goetz, 2009). A new design has been operational since 2014 called the Next Generation Advanced Visible/Infrared Imaging Spectrometer (AVIRIS-NG). The AVIRIS-NG has unprecedented high spectral resolution (5 nm) and high signal-to-noise ratio making it the state-of-the-art of the hyperspectral technology (Chapman et al., 2019). This study uses AVIRIS-NG data recorded at the Rio Tinto mining district (Figure 3) for environmental mapping. A detailed mapping of secondary iron minerals, sulfates, acid water etc., is useful to environmental research concerned with the pollution of the fluvial network that is impacted by acid mine drainage generated at the Rio Tinto mining district. In addition, the results could also be useful for planetary studies related with the remote sensing detection of iron sulfates, iron hydroxides and oxides.

2. Materials and methods

AVIRIS-NG data processing

The AVIRIS-NG images of Rio Tinto mining district were recorded under clear sky condition on June 25, 2021 in 425 narrow spectral bands. The height of the flight was 5.8 km, corresponding to a nominal spatial resolution of 5.2 m. Two AVIRIS-NG scenes cover most of the area of the Rio Tinto mining district. A subset of these two scenes was mosaicked. In Figure 3 is shown an infrared color composite of the AVIRIS-NG image analyzed in this study. The AVIRIS-NG radiance data were converted to surface reflectance using the Fast Line-of-sight Atmospheric Analysis of Hypercubes model (Adler-Golden et al., 1998). The AVIRIS-NG imagery was processed using the spectral mixture analysis (e.g., Roberts et al., 1998; Berman et al., 2004; Adams and Gillespie, 2006; Bedini et al., 2009).

Spectral classes

In the Rio Tinto mining district the sulfide-bearing mine waste and the tailings contain a range of secondary iron-bearing minerals of environmental concern. These secondary minerals form during surface weathering of the sulfides in the waste dumps and tailings. Many of these secondary iron-bearing minerals associated with sulfide-bearing mine waste have distinct electronic and molecular vibrational spectral absorption features (Crowley et al., 2003), including the minerals jarosite [$KFe^{3+}(SO_4)_2(OH)_6$], goethite [$Fe^{3+}O(OH)$], hematite [Fe_2O_3], copiapite [$Fe^{2+}Fe_4^{3+}(SO_4)_6(OH)_2*20H_2O$], melanterite [$Fe^{2+}SO_4*7H_2O$], rozenite [$Fe^{2+}SO_4*4H_2O$], szomolnokite [$Fe^{2+}SO_4*H_2O$]. The secondary iron-bearing minerals are indicators of the pH conditions and the potential for the contamination of the fluvial network (e.g., Crowley et al., 2003). The weathering of sulfides and evaporation processes generate efflorescent salts and saline crusts where also the less soluble minerals gypsum [$CaSO_4*2H_2O$] and jarosite may occur (Pi-Puig et al., 2020; Nieva et al., 2021). Acid waters occur within the mining district in the tailings ponds, in the open pits etc. The fluvial network is impacted from acid mine drainage generated at the Rio Tinto mining district (e.g., Olías et al., 2020; Cánovas et al., 2021; Córdoba et al., 2022). A segment of the Rio Tinto River flows within the study area (Figure 1). The Rio Tinto River contains acid water with very low pH due to contamination from acid mine drainage. The acid waters have characteristic spectral reflectance and can be detected by the analysis of hyperspectral imagery (e.g., Riaza et al., 2015).

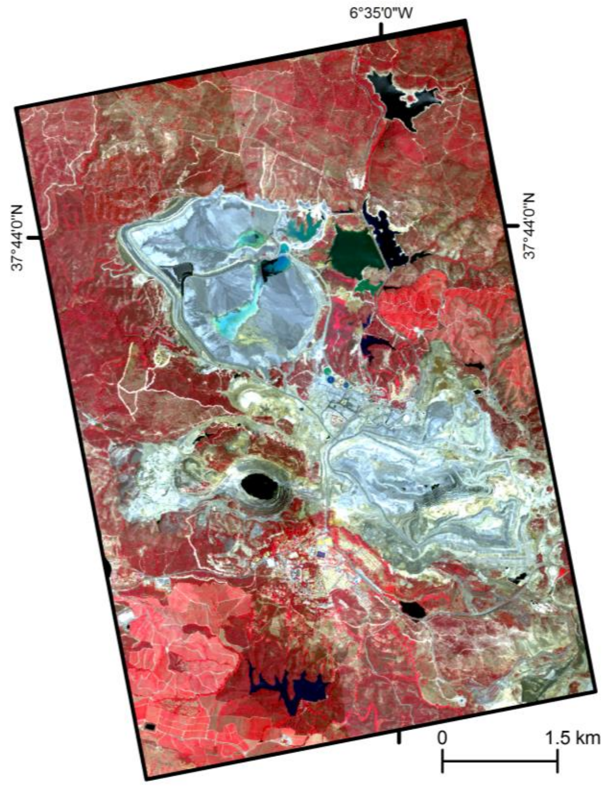

Figure 3. AVIRIS-NG infrared color composite image of the Rio Tinto mining district. The image is a mosaic of two AVIRIS-NG scenes. AVIRIS-NG Band 76 (0.75 μm), red; Band 56 (0.65 μm), green; Band 36 (0.55 μm), blue. In this infrared color composite green vegetation appears in red color.

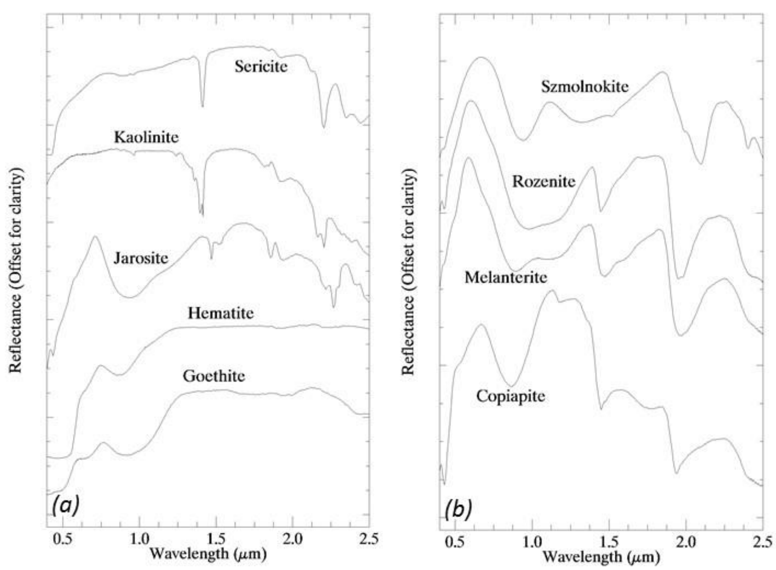

Figure 4. (a) Reflectance spectra of goethite, hematite, jarosite, sericite and kaolinite from the USGS spectral library (Kokaly et al., 2017). (b) Reflectance spectra of several particular iron sulfate hydrate minerals (courtesy of J.K Crowley, USGS).

Sericite and kaolinite are also important spectral classes of the Rio Tinto mining district. These minerals occur in the phyllite rocks or are formed in the hydrothermal alteration processes associated with the sulfide mineralization and surface weathering of feldspars.

Reflectance spectra of the main spectral classes that occur in the Rio Tinto mining district are shown in Figure 4. Reflectance spectra of sericite (muscovite, illite) display an intense Al-OH absorption feature near 2.20 µm (e.g., Clark, 1999; Kokaly et al., 2017). The reflectance spectrum of kaolinite displays a characteristic doublet absorption feature at around 2.17–2.20 µm (e.g., Clark, 1999). Goethite displays a broad ferric iron absorption near 0.92 µm and a peak near 0.75 µm (e.g., Clark, 1999; Kokaly et al., 2017).

Jarosite has a broad ferric iron absorption feature near 0.90 µm and a reflectance maximum at 0.70 µm (Bishop and Murad, 2005). Jarosite displays also diagnostic absorption features in the short wave infrared wavelength region (Figure 4a; Bishop and Murad, 2005). The reflectance spectrum of copiapite (Figure 4b) has a ferric iron broad and deep absorption centered at 0.865 µm and a peak at 0.676 µm. It has high reflectivity between 1.0-1.35 µm, and characteristic water and hydroxyl absorption features at around 1.178 µm, 1.453 µm, 1.768 µm, 1.941 µm and 2.40 µm.

Melanterite is considered the most common ferrous iron sulfate hydrate. The reflectance spectrum of melanterite displays a doublet absorption typical of crystal field transition in ferrous iron with minima located at 0.89 µm and 1.15 µm (Crowley et al., 2003).

Characteristic of melanterite is a reflectance maximum at around 0.58 µm accompanied by strong fall-offs towards the ultraviolet and towards the 0.89 µm absorption feature. Water and hydroxyl absorptions create a typical shape of the reflectance spectrum for the metal sulfate hydrates in the 2.0-2.5 µm wavelength region similar also for rozenite and szomolnokite (Figure 4b). Rozenite has similar spectral features with melanterite but shows a shift toward longer wavelengths of the reflectance maximum at 0.604 µm, and of the ferrous iron doublet absorption at 0.978 µm and 1.17 µm. Szomolnokite displays a reflectance maximum at around 0.67 µm, and ferrous iron absorptions at around 0.94 µm and 1.328 µm. The distinctive absorption at 2.4 µm is attributed to the single water molecule in szomolnokite structure (Crowley et al., 2003). Both rozenite and szomolnokite are dehydration products of melanterite. Gypsum and other Ca-sulfates may also accumulate in the surface of sulfide mine tailings and waste mainly due to evaporation processes. Gypsum reflectance spectra show distinct triplet bands near 1.4–1.5 µm, and multiple features near 2.1–2.3 µm attributed to water (e.g., Bishop et al., 2014).

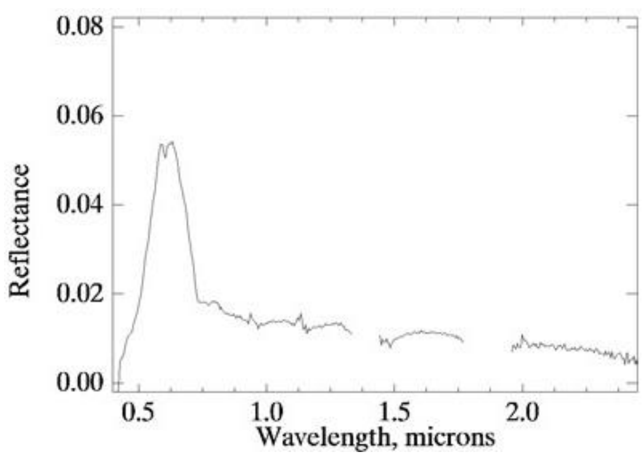

Figure 5. AVIRIS-NG pixel reflectance spectrum over the contaminated water body in the eastern side of the Rio Tinto Mine tailings ponds (*see* Figures 1).

The spectral reflectance of contaminated water is a combination of the spectral properties of water and other infrared active components occurring in it, including solutions and suspended solids. The color of acid water in the river is directly related to the water geochemistry (Sánchez España et al. 2005). Red color acid water is due to the content of iron colloidal Fe(III). Acid waters contaminated by acid mine drainage generated from sulfide-ore mining areas exhibit reflectance spectra that allow their mapping from hyperspectral data (e.g, Figure 5; Riaza et al., 2015). The tailings ponds at Rio Tinto mining district contain acid water on the surface at various locations (Figures 1). The Rio Tinto River, a segment of which flows within the study area (Figure 1), is heavily contaminated by acid mine drainage (Olías et al., 2020).

3. Results and discussion

The results derived from the analysis of the AVIRIS-NG data are shown in Figure 6. The AVIRIS-NG mapped acid water, jarosite, hematite, goethite, undifferentiated metal sulfate hydrates, melanterite/rozenite, copiapite, gypsum, sericite and kaolinite. The acid waters are distinguished at several locations within the Rio Tinto mining district: at the tailings ponds, at the lowest level of the Cerro Colorado open pit, in few areas associated with mine waste, in the Rio Tinto River segment that flows within the study area (Figures 1, 6), etc. The quantity and distribution of the acid waters within the mining district and in the fluvial network is also a function of the season of the year and rainfall (e.g., Olías et al., 2020).

Jarosite is mapped in the mine waste and tailings ponds, and to a less extent in the open pits. Jarosite is an indicator of highly oxidizing, low pH condition, being one of the most common products of sulfide mineral weathering (e.g., Crowley et al., 2003).

Compared to other iron sulfate minerals, jarosite is relatively insoluble and more likely to persist in surface weathering environments (Alpers et al., 1994). Jarosite is mapped in two classes (Figure 6). The first class includes image pixels with purer jarosite reflectance spectra, while jarosite in the second class shows a higher degree of mixtures with goethite, hematite or phyllosilicates. Goethite is the most abundant secondary iron mineral. It is mapped in the rocks exposed on the open pits and in the mine waste dumps. The AVIRIS-NG goethite pixel spectra are often associated with sericite or kaolinite absorption features.

To be noted that the gossan over the sulfide mineralization that has been removed from the open pits has also a goethite reflectance spectrum. In addition, the gossan material has been used in the construction of the tailings ponds, which is the reason of goethite being also mapped in the tailings ponds borders (Figure 6).

Hematite shows a certain spatial association with jarosite-rich areas on the surface of sulfide mine waste dumps. The presence of the meta-stable secondary mineral ferrihydrite [$5Fe_2O_3*9H_2O$], and ferrihydrite-hematite mixtures are also evident in the AVIRIS-NG data. In Figure 6 they are merged in the hematite class. The tailings ponds contain metal sulfate hydrates of various composition and gypsum due to the mineral processing operations and evaporation processes. Large areas of the tailings ponds are mapped in the class "undifferentiated metal sulfate hydrates" (Figure 6). Due to evaporation processes the upper oxidized crust of the tailings consists of mixtures of various Fe, Mg, Al sulfate hydrate minerals and efflorescences (e.g., Valente and Gomes, 2009; Dold, 2014).

Copiapite a mixed valence ferric and ferrous iron sulfate hydrate is identified in small areas of the sulfide-bearing mine waste and in the tailings ponds. Melanterite and its dehydrated varieties rozenite and szomolnokite are detected by the analysis of the airborne hyperspectral AVIRIS-NG image at two localities within the Rio Tinto mining district. AVIRIS-NG pixel spectra of melanterite and rozenite are shown in Figure 7.

These minerals are also present in other areas of the mine waste dumps, at the tailings ponds and banks of the Rio Tinto River (e.g., Roach et al., 2006). However, the 5.2 m spatial resolution of the AVIRIS-NG data and mixtures with other infrared-active minerals (goethite, jarosite, metal sulfate hydrates, efflorescences etc.) may limit the ability of the airborne hyperspectral data to discern individual species of these iron sulfate minerals.

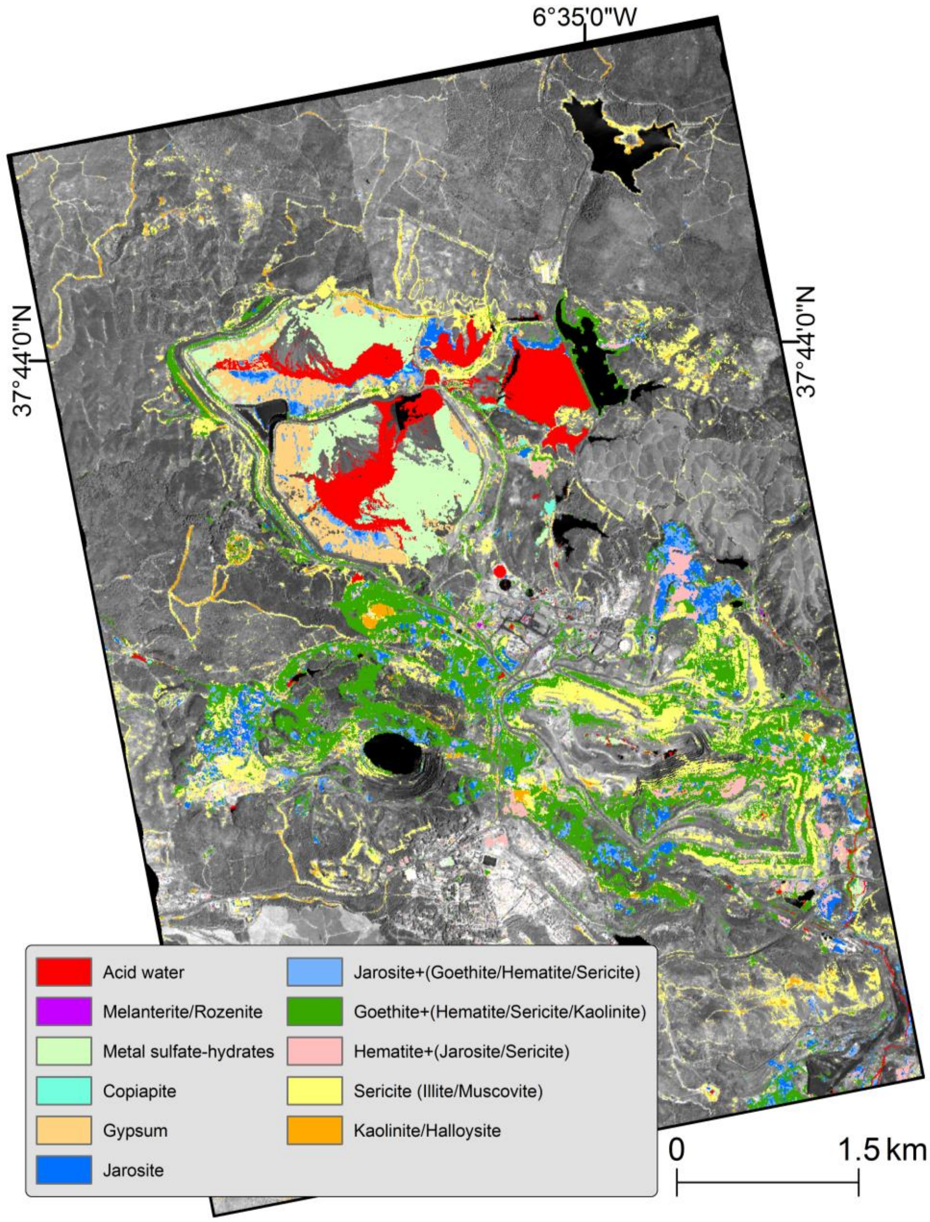

Figure 6. Classified AVIRIS-NG image of the Rio Tinto mining district. The grey scale background image is AVIRIS-NG band 100.

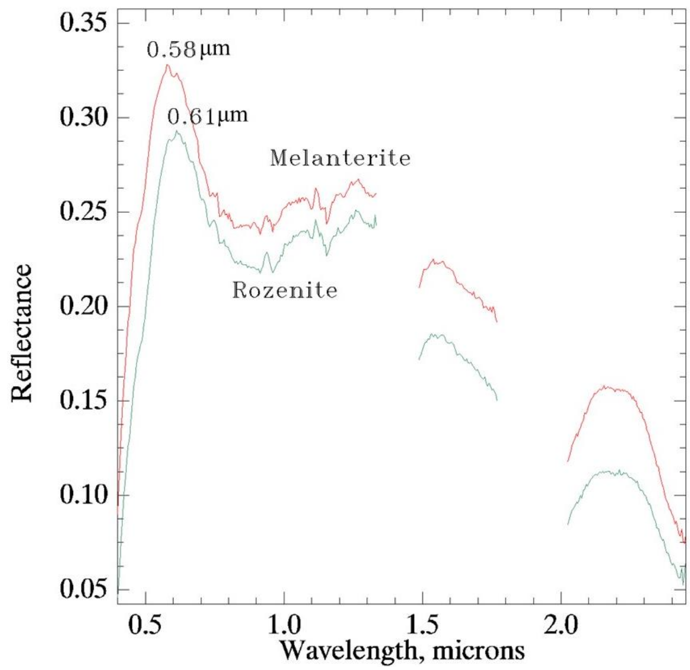

Figure 7. AVIRIS-NG pixel spectra showing the presence of the iron sulfate hydrate minerals melanterite and rozenite. A reflectance maximum at 0.58 µm is typical for melanterite. The reflectance maximum for rozenite is typically at 0.60 µm. Particular chemical composition or a small degree of mixture with szomolnokite may be the cause of the shift of the reflectance maximum to 0.61 µm.

Sericite (muscovite, illite) is abundant as the predominant infrared-active mineral in some areas of the open pits, mine waste dumps, in the unpaved roads etc. There are distinguished sericite reflectance spectra with a strong Al-OH absorption feature around 2.2 µm, and with a weak and shallow Al-OH absorption feature around 2.2 µm. The first class is usually associated with exposed rocks in the open pits. In order to not complicate the readability of the map shown in Figure 6, these classes are merged in one sericite class.

Kaolinite has also been mapped at several locations in the mining district.

4. Conclusions

This study analyzed airborne hyperspectral remote sensing imagery recorded by NASA's AVIRIS-NG sensor over the Rio Tinto mining district in southwestern Spain. The AVIRIS-NG accurately mapped the surface distribution of several infrared-active minerals in the Rio Tinto mining district. The secondary iron minerals jarosite, goethite, hematite, copiapite, melanterite, rozenite, and other metal sulfate hydrates are indicators of the acid mine drainage generation in the Rio Tinto mining district, where large areas covered by sulfide mine waste and tailings of sulfide ore processing occur. Acid water was also distinguished from its characteristic spectral reflectance properties in a segment of the Rio Tinto River that flows within the study area, at the tailings ponds and in other small zones within the mining district. The mapping results produced by the analysis of the AVIRIS-NG data can be useful to the environmental studies concerned with the pollution from acid mine drainage of the fluvial network of the area. The study can also serve as a guidance for the analysis of satellite hyperspectral data in environmental applications.

Acknowledgment

The AVIRIS-NG data of the Rio Tinto mining district were made available from the Jet Propulsion Laboratory (JPL) of NASA, USA. https://www.jpl.nasa.gov/.

References

Adams, J.B. and Gillespie, A.R., 2006. Remote sensing of landscapes with spectral images: A physical modeling approach. Cambridge University Press.

Adler-Golden, S., Berk, A., Bernstein, L.S., Richtsmeier, S., Acharya, P.K., Matthew, M.W., Anderson, G.P., Allred, C.L., Jeong, L.S. and Chetwynd, J.H., 1998. FLAASH, a MODTRAN4 atmospheric correction package for hyperspectral data retrievals and simulations. In Proc. 7th Ann. JPL Airborne Earth Science Workshop (Vol. 97, pp. 9-14). Pasadena, CA: JPL Publication.

Alpers, C.N., Blowes, D.W., Nordstrom, D.K. and Jambor, J.L., 1994. Secondary minerals and acid mine-water chemistry. In: Jambor, J.L. and Blowes, D.W. (eds.) Short Course Handbook on Environmental Geochemistry of Sulfide Mine-Wastes. Mineralogical Association of Canada, Waterloo, Ontario, 247–270.

Amils, R., González-Trill, E., Fernández-Remolar, D., Gómez, F., Aguilera, Á., Rodríguez, N., Malki, M., García-Moyano, A., Fairén, A.G., de la Fuente, V. and Sanz, J.L., 2007. Extreme environments as Mars terrestrial analogs: The Rio Tinto case. Planetary and Space Science, 55, 370-381.

Antón-Pacheco, C., Rowan, L.C., Mars, J.C. and Gumiel, J.C., 2001. Characterization of mine waste materials and hydrothermally altered rocks in the Rio Tinto mining district (southwest Spain) using Hymap data. Revista de Teledetección, 16, 65-68.

Bedini, E., 2017. The use of hyperspectral remote sensing for mineral exploration: A review. Journal of Hyperspectral Remote Sensing, 7(4), 189-211.

Bedini, E., van der Meer, F. and van Ruitenbeek, F., 2009. Use of HyMap imaging spectrometer data to map mineralogy in the Rodalquilar caldera, southeast Spain. International Journal of Remote Sensing, 30, 327-348.

Berman, M., Kiiveri, H., Lagerstrom, R., Ernst, A., Dunne, R. and Huntington, J.F., 2004. ICE: A statistical approach to identifying endmembers in hyperspectral images. IEEE Transactions on Geoscience and Remote Sensing, 42, 2085-2095.

Bishop, J.L., Lane, M.D., Dyar, M.D., King, S.J., Brown, A.J. and Swayze, G.A., 2014. Spectral properties of Ca-sulfates: Gypsum, bassanite, and anhydrite. American Mineralogist, 99, 2105-2115.

Bishop, J.L. and Murad, E., 2005. The visible and infrared spectral properties of jarosite and alunite. American Mineralogist, 90, 1100-1107.

Buckby, T., Black, S., Coleman, M.L. and Hodson, M.E., 2003. Fe-sulphate-rich evaporative mineral precipitates from the Rio Tinto, southwest Spain. Mineralogical Magazine, 67, 263-278.

Cánovas, C.R., Macías, F., Basallote, M.D., Olías, M., Nieto, J.M. and Pérez-López, R., 2021. Metal (loid) release from sulfide-rich wastes to the environment: the case of the Iberian Pyrite Belt (SW Spain). Current Opinion in Environmental Science & Health, 20, p.100240.

Carter, J., Poulet, F., Murchie, S. and Bibring, J.P., 2013. Automated processing of planetary hyperspectral datasets for the extraction of weak mineral signatures and applications to CRISM observations of hydrated silicates on Mars. Planetary and Space Science, 76, 53-67.

Chapman, J.W., Thompson, D.R., Helmlinger, M.C., Bue, B.D., Green, R.O., Eastwood, M.L., Geier, S., Olson-Duvall, W. and Lundeen, S.R., 2019. Spectral and radiometric calibration of the next generation airborne visible infrared spectrometer (AVIRIS-NG). Remote Sensing, 118, p. 2129.

Choe, E., van der Meer, F., van Ruitenbeek, F., van der Werff, H., de Smeth, B. and Kim, K.W., 2008. Mapping of heavy metal pollution in stream sediments using combined geochemistry, field spectroscopy, and hyperspectral remote sensing: A case study of the Rodalquilar mining area, SE Spain. Remote Sensing of Environment, 112, 3222-3233.

Clark, R.N. Spectroscopy of Rocks and Minerals, and Principles of Spectroscopy, in: A. Rencz (Ed.), Manual of Remote Sensing vol. 3. Wiley and Sons Inc., New York, pp. 3-58, 1999.

Córdoba, F., Luís, A.T., Leiva, M., Sarmiento, A.M., Santisteban, M., Fortes, J.C., Dávila, J.M., Álvarez-Bajo, O. and Grande, J.A., 2022.

Biogeochemical indicators (waters/diatoms) of acid mine drainage pollution in the Odiel river (Iberian Pyritic Belt, SW Spain). Environmental Science and Pollution Research, 12 p.

Crowley, J.K., Williams, D.E., Hammarstrom, J.M., Piatak, N., Chou, I.M. and Mars, J.C., 2003. Spectral reflectance properties (0.4–2.5 μm) of secondary Fe-oxide, Fe-hydroxide, and Fe-sulphate-hydrate minerals associated with sulphide-bearing mine wastes. Geochemistry: Exploration, Environment, Analysis, 3, 219-228.

Dold, B., 2014. Evolution of acid mine drainage formation in sulphidic mine tailings. Minerals, 4, 621-641.

Elghali, A., Benzaazoua, M., Bouzahzah, H., Bussière, B. and Villarraga-Gómez, H., 2018. Determination of the available acid-generating potential of waste rock, part I: Mineralogical approach. Applied Geochemistry, 99, 31-41.

Sánchez España, J., Pamo, E.L., Santofimia, E., Aduvire, O., Reyes, J. and Barettino, D., 2005. Acid mine drainage in the Iberian Pyrite Belt (Odiel river watershed, Huelva, SW Spain): geochemistry, mineralogy and environmental implications. Applied geochemistry, 20, 1320-1356.

Farrand, W.H. and Bhattacharya, S., 2021. Tracking Acid Generating Minerals and Trace Metal Spread from Mines using Hyperspectral Data: Case Studies from Northwest India. International Journal of Remote Sensing, 42, 2920-2939.

Fernández-Remolar, D.C., Morris, R.V., Gruener, J.E., Amils, R. and Knoll, A.H., 2005. The Río Tinto Basin, Spain: mineralogy, sedimentary geobiology, and implications for interpretation of outcrop rocks at Meridiani Planum, Mars. Earth and Planetary Science Letters, 240, 149-167.

Goetz, A.F., 2009. Three decades of hyperspectral remote sensing of the Earth: A personal view. Remote Sensing of Environment, 113, S5-S16.

Kokaly, R.F., Clark, R.N., Swayze, G.A., Livo, K.E., Hoefen, T.M., Pearson, N.C., Wise, R.A., Benzel, W.M., Lowers, H.A., Driscoll, R.L. and Klein, A.J., 2017. USGS spectral library version 7 data: Us Geological Survey data release. United States Geological Survey (USGS): Reston, VA, USA.

Kruse, F.A., 2012. Mapping surface mineralogy using imaging spectrometry. Geomorphology, 137, 41-56.

Kopačková, V. and Hladíková, L., 2014. Applying spectral unmixing to determine surface water parameters in a mining environment. Remote Sensing, 6, 11204-11224.

Liu, Y., Glotch, T.D., Scudder, N.A., Kraner, M.L., Condus, T., Arvidson, R.E., Guinness, E.A., Wolff, M.J. and Smith, M.D., 2016. End-member identification and spectral mixture analysis of CRISM hyperspectral data: A case study on southwest Melas Chasma, Mars. Journal of Geophysical Research: Planets, 121, 2004-2036.

Nieva, N.E., Garcia, M.G., Borgnino, L. and Borda, L.G., 2021. The role of efflorescent salts associated with sulfide-rich mine wastes in the short-term cycling of arsenic: Insights from XRD, XAS, and μ-XRF studies. Journal of Hazardous Materials, 404, 124158.

Olías, M., Cánovas, C.R., Macías, F., Basallote, M.D. and Nieto, J.M., 2020. The evolution of pollutant concentrations in a river severely affected by acid mine drainage: Río Tinto (SW Spain). Minerals, 10, p.598.

Olías, M., Nieto, J.M., 2015. Background conditions and mining pollution throughout history in the Río Tinto (SW Spain). Environments, 2, 295–316.

Olías, M., Nieto, J.M., Sarmiento, A.M., Cánovas, C.R. and Galván, L., 2011. Water quality in the future Alcolea reservoir (Odiel River, SW Spain): a clear example of the inappropriate management of water resources in Spain. Water resources management, 25, 201-215.

Pascual, E., Donaire, T., Toscano, M., Macías, G., Pin, C. and Hamilton, M.A., 2021. Geochemical and Volcanological Criteria in Assessing the Links between Volcanism and VMS Deposits: A Case on the Iberian Pyrite Belt, Spain. Minerals, 11, p.826.

Pi-Puig, T., Solé, J. and Gómez Cruz, A., 2020. Mineralogical Study and Genetic Model of Efflorescent Salts and Crusts from Two Abandoned Tailings in the Taxco Mining District, Guerrero (Mexico). Minerals, 10, p.871

Riaza, A., Buzzi, J., Garcia-Melendez, E., Carrère, V., Sarmiento, A. and Müller, A., 2015. Monitoring acidic water in a polluted river with hyperspectral remote sensing (HyMap). Hydrological Sciences Journal, 60, 1064-1077.

Riaza, A., Buzzi, J., García-Meléndez, E., Carrère, V. and Müller, A., 2011. Monitoring the extent of contamination from acid mine drainage in the Iberian Pyrite Belt (SW Spain) using hyperspectral imagery. Remote Sensing, 3, 2166-2186.

Roach, L.H., Mustard, J., Gendrin, A., Fernández-Remolar, D., Amils, R. and Amaral-Zettler, L., 2006. Finding mineralogically interesting targets for exploration from spatially coarse visible and near IR spectra. Earth and Planetary Science Letters, 252, 201-214.

Roberts, D.A., Gardner, M., Church, R., Ustin, S., Scheer, G. and Green, R.O., 1998. Mapping chaparral in the Santa Monica Mountains using multiple endmember spectral mixture models. Remote sensing of environment, 65(3), pp.267-279.

Rull, F., Veneranda, M., Manrique-Martinez, J.A., Sanz-Arranz, A., Saiz, J., Medina, J., Moral, A., Perez, C., Seoane, L., Lalla, E. and Charro, E., 2021. Spectroscopic study of terrestrial analogues to support rover missions to Mars–A Raman-centred review. Analytica Chimica Acta, p.339003.

Sobron, P., Bishop, J.L., Blake, D.F., Chen, B. and Rull, F., 2014. Natural Fe-bearing oxides and sulfates from the Rio Tinto Mars analog site: Critical assessment of VNIR reflectance spectroscopy, laser Raman spectroscopy, and XRD as mineral identification tools. American Mineralogist, 99, 1199-1205.

Swayze, G.A., Smith, K.S., Clark, R.N., Sutley, S.J., Pearson, R.M., Vance, J.S., Hageman, P.L., Briggs, P.H., Meier, A.L., Singleton, M.J. and Roth, S., 2000. Using imaging spectroscopy to map acidic mine waste. Environmental Science & Technology, 34, 47-54.

de la Torre, M.L., Grande, J.A., Graiño, J., Gómez, T. and Cerón, J.C., 2011. Characterization of AMD pollution in the river Tinto (SW Spain). Geochemical comparison between generating source and receiving environment. Water, Air, & Soil Pollution, 216, 3-19.

Valente, T.M. and Gomes, C.L., 2009. Occurrence, properties and pollution potential of environmental minerals in acid mine drainage. Science of the Total Environment, 407, 1135-1152.

Williams, D.J., Bigham, J.M., Cravotta, I., C.A., Trainaa, S.J., Anderson, J.E. and Lyon, J.G., 2002. Assessing mine drainage pH from the color and spectral reflectance of chemical precipitates. Applied Geochemistry, 17, 1273-1286.

Young, P.L., 1997. The longevity of minewater pollution: a basis for decision-making. Science of the Total Environment, 194, 457-466.

Zabcic, N., Rivard, B., Ong, C. and Müller, A., 2014. Using airborne hyperspectral data to characterize the surface pH and mineralogy of pyrite mine tailings. International Journal of Applied Earth Observation and Geoinformation, 32, 152-162.